# CMS Physics Analysis Summary

Contact: cms-pag-conveners-susy@cern.ch 2015/12/15

# Search for supersymmetry in the multijet and missing transverse momentum channel in pp collisions at 13 TeV

The CMS Collaboration

## Abstract

A search for new physics is performed based on multijet events with large missing transverse momentum produced in proton-proton collisions at $\sqrt{s} = 13$ TeV. The data sample, corresponding to an integrated luminosity of 2.2 $\text{fb}^{-1}$, was collected with the CMS detector at Run 2 of the CERN LHC. The data are examined in search regions of jet multiplicity, bottom-quark jet multiplicity, missing transverse momentum, and the scalar sum of jet transverse momenta. The observed numbers of events in all search regions are found to be consistent with the expectations from standard model processes. Exclusion limits are presented for simplified supersymmetric models of gluino pair production. For a scenario in which both gluinos decay to a bottom quark-antiquark pair and to a stable, massless, weakly interacting, lightest neutralino, gluinos with mass below 1600 GeV are excluded. For the corresponding scenarios with a top quark-antiquark pair or with a generic quark-antiquark pair in place of the bottom quark-antiquark pair, the respective limits are 1530 and 1440 GeV. These results significantly extend the limits from LHC Run 1.

# 1 Introduction

The standard model (SM) of particle physics successfully describes a wide range of phenomena. However, in the SM, the Higgs boson mass is unstable to higher-order corrections, suggesting that the SM is incomplete. Many extensions to the SM have been proposed to provide a more fundamental theory. Supersymmetry (SUSY) [1–8], one such extension, postulates that each SM particle is paired with a SUSY partner from which it differs in spin by one-half unit. As examples, squarks and gluinos are the SUSY partners of quarks and gluons, respectively. Radiative corrections involving SUSY particles can compensate the contributions from SM particles and thereby stabilize the Higgs boson mass. For this cancellation to be "natural" [9–11], the top squark, bottom squark, and gluino must have masses on the order of 1 TeV or less, possibly allowing them to be produced at the CERN LHC.

Amongst SUSY processes, gluino pair production, typically yielding four or more hadronic jets in the final state, has the largest potential cross section, making it an apt channel for early SUSY searches at the recently started LHC Run 2. Furthermore, in R-parity [12] conserving SUSY models, as are considered here, the lightest SUSY particle (LSP) is stable and assumed to be weakly interacting, leading to potentially large undetected, or "missing", transverse momentum $\vec{p}_{\mathrm{T}}^{\,\mathrm{miss}}$. Supersymmetry events at the LHC might thus be characterized by significant $\vec{p}_{\mathrm{T}}^{\,\mathrm{miss}}$, numerous jets, and – in the context of natural SUSY – jets initiated by top and bottom quarks.

This document describes a search for natural SUSY in the all-hadronic final state. The data, corresponding to 2.2 $\mathrm{fb}^{-1}$ of proton-proton collisions at $\sqrt{s} = 13\,\mathrm{TeV}$, were collected with the CMS detector at the LHC Run 2. Because of their all-hadronic nature, the SUSY events are expected to exhibit large values of $H_{\mathrm{T}}$, where $H_{\mathrm{T}}$ is the scalar sum of the transverse momentum values ($p_{\mathrm{T}}$) of the jets. We present a general search for gluino pair production leading to final states with large $\vec{p}_{\mathrm{T}}^{\,\mathrm{miss}}$, large $H_{\mathrm{T}}$, and large jet multiplicity. The data are examined in bins of $N_{\mathrm{jet}}$, $N_{\text{b-jet}}$, $H_{\mathrm{T}}$, and $H_{\mathrm{T}}^{\mathrm{miss}}$, where $N_{\mathrm{jet}}$ is the number of jets, $N_{\text{b-jet}}$ the number of tagged bottom-quark jets (b jets), and $H_{\mathrm{T}}^{\mathrm{miss}}$– used as a measure of $\vec{p}_{\mathrm{T}}^{\,\mathrm{miss}}$ – the magnitude of the vector sum of the jet transverse momenta. The search is performed in exclusive bins of these four observables.

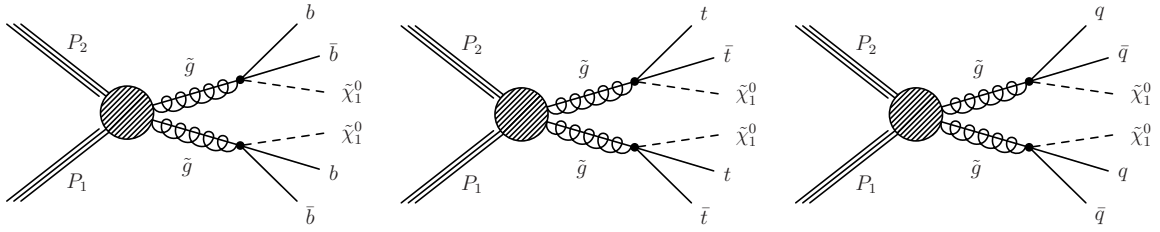


Figure 1: Event diagrams for the SUSY scenarios considered in this study: the (left) T1bbbb, (center) T1tttt, and (right) T1qqqq simplified model spectra scenarios, with $\tilde{\chi}_1^0$ the lightest neutralino, taken to be weakly interacting and stable.

As SUSY scenarios, we consider simplified model spectra [13–16] in which gluino pair production is followed by the decay of each gluino into a bottom quark and an off-shell bottom squark [Fig. 1 (left)] or into a top quark and an off-shell top squark [Fig. 1 (center)]. The off-shell bottom (top) squark decays into a bottom (top) quark and the LSP, where the LSP is assumed to escape detection, leading to significant $\vec{p}_{\mathrm{T}}^{\,\mathrm{miss}}$. We also consider the corresponding generic scenario in which any flavor of quark can be produced [Fig. 1 (right)]. We denote the three possibilities the T1bbbb, the T1tttt, and the T1qqqq scenarios, respectively [17]. If the bottom (top) squark is much lighter than any other squark but heavier than the gluino, gluino decays are expected to be dominated by the three-body process of Fig. 1 (left) [1 (center)]. In SUSY models, a fa-

vored LSP candidate is the lightest neutralino state $\widetilde{\chi}_1^0$, where a neutralino is a mixture of the SUSY partners of Higgs and gauge bosons; we therefore use the symbol $\widetilde{\chi}_1^0$ to denote the LSP. We assume all SUSY particles other than the gluino and the LSP to be too heavy to be directly produced, and the gluino to be short-lived.

The principal sources of background arise from the SM production of top quarks [mostly from top quark-antiquark ($\mathrm{t\bar{t}}$) pair production but also from single-top quark processes], a W or Z boson in association with jets (W+jets or Z+jets events, where the W and Z bosons can be either on- or off-shell), and multiple jets through the strong interaction [quantum chromodynamics (QCD) multijet production]. For top-quark and W+jets events, significant $\vec{p}_{\mathrm{T}}^{\,\mathrm{miss}}$ can arise if a W boson decays leptonically, producing a neutrino, while Z+jets events can exhibit significant $\vec{p}_{\mathrm{T}}^{\,\mathrm{miss}}$ if the Z boson decays to two neutrinos. For QCD multijet events, significant $\vec{p}_{\mathrm{T}}^{\,\mathrm{miss}}$ can arise if the event contains a charm or bottom quark that undergoes semileptonic decay, but the principal source of $\vec{p}_{\mathrm{T}}^{\,\mathrm{miss}}$ is the mismeasurement of jet $p_{\mathrm{T}}$.

This study combines and extends search strategies developed for the analysis of the CMS Run 1 data at $\sqrt{s} = 8\,\mathrm{TeV}$, specifically the study of Ref. [18], which examined data in bins of $N_{\text{b-jet}}$ but not $N_{\text{jet}}$ and proved sensitive to the T1bbbb scenario, and the study of Ref. [19], which examined data in bins of $N_{\text{jet}}$ but not $N_{\text{b-jet}}$ and proved sensitive to the T1tttt and T1qqqq scenarios. Here, the two approaches are combined in a unified framework to yield a more comprehensive and inclusive study with improved sensitivity.

## 2 Detector, trigger, and event reconstruction

The CMS detector is built around a superconducting solenoid of 6 m internal diameter, providing a magnetic field of 3.8 T. Within the superconducting solenoid volume are a silicon pixel and strip tracker, a lead-tungstate crystal electromagnetic calorimeter (ECAL), and a brass and scintillator hadron calorimeter (HCAL). The ECAL and HCAL, each composed of a barrel and two endcap sections, extend over a pseudorapidity [20] range $|\eta| < 3.0$. The tracking chambers cover $|\eta| < 2.5$. Forward calorimeters on each side of the interaction point encompass $3.0 < |\eta| < 5.0$. Muons are measured within $|\eta| < 2.4$ by gas-ionization detectors embedded in the steel flux-return yoke outside the solenoid. The detector is nearly hermetic, permitting accurate measurements of $\vec{p}_{\mathrm{T}}^{\,\mathrm{miss}}$. A more detailed description of the CMS detector, together with a definition of the coordinate system and relevant kinematic variables, is given in Ref. [20].

Signal event candidates are recorded using trigger conditions based on thresholds on $H_{\mathrm{T}}$ and $|\vec{p}_{\mathrm{T}}^{\,\mathrm{miss}}|$. The trigger efficiency, which exceeds 98% following application of the event selection criteria described below, is measured in data and is accounted for in the analysis. Separate data samples requiring the presence of either charged leptons or photons are used for the determination of backgrounds from SM processes, as described below.

Physics objects are defined using the particle-flow (PF) algorithm [21, 22], which reconstructs and identifies individual particles through an optimized combination of information from different detector components. The PF candidates are classified as photons, charged hadrons, neutral hadrons, electrons, or muons. The event primary vertex is taken to be the reconstructed vertex with the largest sum of charged-track $p_{\mathrm{T}}^2$ values and is required to lie within 24 cm (2 cm) of the center of the detector in the direction along (perpendicular to) the beam axis. Charged tracks from extraneous pp interactions within the same or a nearby bunch crossing ("pileup") are removed [23]. The PF objects serve as input for jet reconstruction, based on the anti-$k_{\mathrm{T}}$ algorithm [24, 25] with a distance parameter of 0.4. Contributions to an individual jet's $p_{\mathrm{T}}$ from pileup interactions are subtracted [26], and corrections are applied as a function of jet $p_{\mathrm{T}}$ and $\eta$

to account for residual effects of non-uniform detector response [27].

The identification of b jets is performed using the combined secondary vertex algorithm at the medium working point [28, 29]. The b-tagging efficiency and mistag probability are measured from data control samples as a function of jet $p_T$ and $\eta$. The average signal efficiency for b jets (misidentification probability for light-quark and gluon jets) is approximately 70% (1.5%) for jet $p_T > 60\,\text{GeV}$ [29].

Jets, including b jets, must have $p_T > 30\,\text{GeV}$ and satisfy quality criteria [27] that reject spurious signals from calorimeter noise.

Electrons and muons are required to be isolated. The isolation criterion is based on the variable $I_{\text{iso}}$, which is the scalar sum of the $p_T$ values of all PF charged hadrons, neutral hadrons, and photons within a cone of radius $R_{\text{cone}} = \sqrt{(\Delta\phi)^2 + (\Delta\eta)^2}$ around the lepton direction, divided by the lepton $p_T$. The sum excludes the lepton under consideration and is corrected for the contribution of pileup. The cone radius is $R_{\text{cone}} = 0.2$ for lepton $p_T \leq 50\,\text{GeV}$, $R_{\text{cone}} = 10\,\text{GeV}/p_T$ for lepton $50 \leq p_T \leq 200\,\text{GeV}$, and $R_{\text{cone}} = 0.05$ for lepton $p_T \geq 200\,\text{GeV}$. The reason for the decrease in $R_{\text{cone}}$ with increasing $p_T$ is to account for the increased collimation of a heavy particle's decay products as the object becomes more boosted. We require $I_{\text{iso}} < 0.1$ for electrons and $I_{\text{iso}} < 0.2$ for muons.

Charged tracks not identified as an isolated electron or muon are also subjected to an isolation criterion. To be considered an isolated charged-particle track, the scalar sum of charged-track $p_T$ values (excluding the track under consideration) in a cone of radius $R_{\text{cone}} = 0.3$ around the track direction, divided by the track $p_T$, must be less than 0.2 if the track is identified by the PF procedure as electron or muon, and less than 0.1 otherwise.

## 3 Event selection and search regions

The following requirements define the selection criteria for signal event candidates:

- $N_{\text{jet}} \geq 4$, where the jets must satisfy $|\eta| < 2.4$; we require at least four jets because of our focus on gluino pair production;
- $H_T > 500\,\text{GeV}$, where $H_T$ is the scalar $p_T$ sum of jets with $|\eta| < 2.4$;
- $H_T^{\text{miss}} > 200\,\text{GeV}$, where $H_T^{\text{miss}}$ is the magnitude of the vector $p_T$ sum of jets with $|\eta| < 5$; the $\eta$ range is extended in this case to improve the $\vec{p}_T^{\,\text{miss}}$ measurement;
- no identified, isolated electron or muon candidate with $p_T > 10\,\text{GeV}$; electron candidates are restricted to $|\eta| < 2.5$ and muon candidates to $|\eta| < 2.4$, and muon candidates must have a distance of closest approach to the primary vertex less than 0.5 mm in the direction along the beam axis and 0.2 mm in the transverse plane;
- no isolated charged-particle track with $|\eta| < 2.4$, $m_T < 100\,\text{GeV}$, and $p_T > 10\,\text{GeV}$ ($p_T > 5\,\text{GeV}$ if the track is identified as an electron or muon candidate by the PF algorithm), where $m_T$ is the transverse mass [30] formed from the $\vec{p}_T^{\,\text{miss}}$ and isolated-track $p_T$ vectors, with $\vec{p}_T^{\,\text{miss}}$ defined by the projection onto the transverse plane of the negative of the vector sum of all PF objects;
- $\Delta\phi_{H_T^{\text{miss}},j_i} > 0.5$ ($> 0.3$) for the two highest $p_T$ jets $j_1$ and $j_2$ (the next two highest $p_T$ jets $j_3$ and $j_4$), with $\Delta\phi_{H_T^{\text{miss}},j_i}$ the angle between the $H_T^{\text{miss}}$ vector and the $p_T$ vector of jet $j_i$.

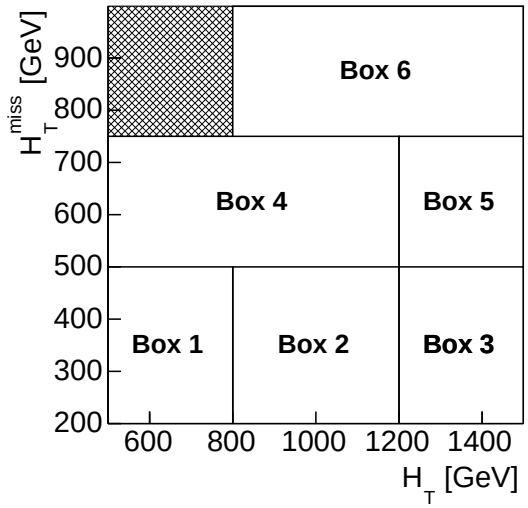


Figure 2: Schematic illustration of the search intervals in the $H_{\mathrm{T}}^{\mathrm{miss}}$ versus $H_{\mathrm{T}}$ plane. Each of the six $H_{\mathrm{T}}$ and $H_{\mathrm{T}}^{\mathrm{miss}}$ intervals is examined as a function of three $N_{\mathrm{jet}}$ bins and four $N_{\text{b-jet}}$ bins for a total of 72 search regions.

The isolated-track requirement eliminates events with a hadronically decaying $\tau$ lepton as well as isolated electrons or muons in cases where the lepton is not identified; the $m_{\mathrm{T}}$ requirement restricts this veto to tracks consistent with W boson decay in order to minimize the impact on signal efficiency. The $\Delta\phi_{H_{\mathrm{T}}^{\mathrm{miss}},j_i}$ requirements reduce the background from QCD multijet processes, for which $\vec{p}_{\mathrm{T}}^{\,\mathrm{miss}}$ is usually aligned along a jet direction.

The search is performed in the following exclusive intervals of the four search variables:

- $N_{\mathrm{jet}}$: $4-6$, $7-8$, $\geq 9$;
- $N_{\text{b-jet}}$: 0, 1, 2, $\geq 3$;
- $H_{\mathrm{T}}$: $500-800$, $800-1200$, $\geq 1200\,\mathrm{GeV}$;
- $H_{\mathrm{T}}^{\mathrm{miss}}$: $200-500$, $500-750$, $\geq 750\,\mathrm{GeV}$.

The bins with $H_{\mathrm{T}} < 800\,\mathrm{GeV}$ and $H_{\mathrm{T}}^{\mathrm{miss}} > 750\,\mathrm{GeV}$ are discarded because $H_{\mathrm{T}}^{\mathrm{miss}}$ cannot exceed $H_{\mathrm{T}}$ in a physical event. Additionally, for $500 < H_{\mathrm{T}}^{\mathrm{miss}} < 750\,\mathrm{GeV}$, an expanded interval $500 < H_{\mathrm{T}} < 1200\,\mathrm{GeV}$ is used, and for $H_{\mathrm{T}}^{\mathrm{miss}} > 750\,\mathrm{GeV}$ a single interval $H_{\mathrm{T}} > 800\,\mathrm{GeV}$, because of the lower expected number of events at large $H_{\mathrm{T}}^{\mathrm{miss}}$. The six search intervals in the $H_{\mathrm{T}}^{\mathrm{miss}}$ versus $H_{\mathrm{T}}$ plane are illustrated schematically in Fig. 2. The total number of search regions is 72.

# 4 Event simulation

The background is evaluated using data control samples, as described in Section 5. Simulated samples of SM events are used to construct and validate the procedures. For this latter purpose, the MADGRAPH5 [31] event generator is used to simulate $\mathrm{t\bar{t}}$, W+jets, Z+jets, $\gamma$ + jets, and QCD multijet events. Single-top events in the $t$ and tW channels are described using the POWHEG v1.0 [32–36] program, and in the $s$ channel using the MADGRAPH5_aMC@NLO [37] program. The latter generator is also used to simulate events with dibosons (WW, ZZ, and WH production, etc., with H a Higgs boson) and rare processes ($\mathrm{t\bar{t}W}$, $\mathrm{t\bar{t}Z}$, and WWZ combinations, etc.), except that POWHEG [38] is used for WW events in which both W bosons decay leptoni-

cally. Simulation of the detector response is based on the GEANT4 [39] package. The simulated samples are normalized using the most accurate cross section calculations currently available, generally with next-to-next-to-leading-order accuracy.

Signal T1bbbb, T1tttt, and T1qqqq events are simulated for a range of gluino $m_{\tilde{g}}$ and LSP $m_{\tilde{\chi}_1^0}$ mass values, with $m_{\tilde{\chi}_1^0} < m_{\tilde{g}}$. The signal samples are based on the MADGRAPH generator, with up to two partons present in addition to the gluino pair. The decays of the gluino are described with a pure phase-space matrix element [40]. The signal production cross sections are computed [41–45] with next-to-leading order (NLO) plus next-to-leading-logarithm (NLL) accuracy. To reduce computational requirements, the detector is modeled with the CMS fast simulation program [46, 47], which yields consistent results compared with the GEANT4-based simulation.

The NNPDF3.0LO [48] parton distribution functions (PDF) are used for the MADGRAPH signal and background samples, and the NNPDF3.0NLO [48] PDFs for the POWHEG and MADGRAPH5_aMC@NLO samples. All simulated samples use the PYTHIA 8.2 [40] program to describe parton showering and hadronization. To model the effects of pileup, the simulated events are generated with a nominal distribution of pp interactions per bunch crossing and then reweighted to match the corresponding distribution in data.

Table 1: Summary of systematic uncertainties that affect the signal event selection efficiency.

| Item | Relative uncertainty (%) |
|---|---|
| Integrated luminosity | 4.6 |
| Trigger efficiency | 1.1 |
| Pileup reweighting | 0.5 |
| Parton distribution functions | 10 |
| Renormalization and factorization scales | 0–3 |
| Initial-state radiation | 0-11 |
| Jet energy scale | 0.5–4 |
| Isolated-lepton and -track vetoes (T1tttt only) | 2 |

We evaluate systematic uncertainties in the signal model predictions. Those that are relevant for the selection efficiency are listed in Table 1. The uncertainty associated with the renormalization and factorization scales is determined by varying each scale independently by factors of 2 and 0.5 [49, 50]. An uncertainty related to the modeling of initial-state radiation is determined using the techniques described in Ref. [51]. The uncertainties associated with the renormalization and factorization scales, and with initial-state radiation are typically below 0.1% but can be as large as 1–3, and 3-11%, respectively, for $m_{\tilde{\chi}_1^0} \approx m_{\tilde{g}}$. As a conservative estimate of the uncertainty associated with the PDFs, we consider the change in the signal yield observed for 100 variations of the PDFs, as provided by the NNPDF program, and assign an uncorrelated uncertainty of 10% to each search region. The uncertainty associated with the jet energy scale is evaluated as a function of jet $p_T$ and $\eta$. Note that the isolated-lepton and -track vetoes do not affect the T1bbbb and T1qqqq samples since events in these samples rarely contain an isolated charged track.

Besides the signal efficiency, all the systematic terms in Table 1 except those associated with the integrated luminosity, PDFs, and isolated-lepton and -track vetoes also affect the shapes of the signal distributions, i.e., can cause a migration of events between signal regions.

We also evaluate systematic uncertainties in the signal predictions related to the b-jet tagging

and misidentification efficiencies and to the statistical uncertainties in the signal event samples. These latter two sources of uncertainty do not affect the signal efficiency but can potentially alter the signal shapes.

# 5 Background evaluation

## 5.1 Background from top and W+jets events

Background from SM $\mathrm{t\bar{t}}$, single-top, and W+jets events arises when a W boson decays leptonically, yielding a neutrino (thus, genuine $H_{\mathrm{T}}^{\mathrm{miss}}$) and a non-vetoed charged lepton. The non-vetoed lepton can be an electron or muon (including from $\tau$-lepton decay) that does not satisfy the identification requirements of Section 3 (so-called "lost leptons"), or it can be a hadronically decaying $\tau$ lepton.

### 5.1.1 Lost-lepton background

Lost-lepton background can arise if an electron or muon lies outside the analysis acceptance, is not isolated, or is not reconstructed. The lost-lepton background is evaluated following the procedures described in Refs. [19, 52, 53]. Briefly, single-lepton data control samples (CS) are selected by inverting the electron and muon vetoes. Each CS event is entered into one of the 72 search regions with a weight that represents the probability for a lost-lepton event to appear with the corresponding values of $H_{\mathrm{T}}$, $H_{\mathrm{T}}^{\mathrm{miss}}$, $N_{\mathrm{jet}}$, and $N_{\mathrm{b\text{-}jet}}$.

The control samples are selected by requiring events to satisfy the criteria of Section 3 except exactly one isolated electron or muon must be present and the isolated-track veto is not applied. The transverse mass formed from the $\vec{p}_{\mathrm{T}}^{\,\mathrm{miss}}$ and lepton-$p_{\mathrm{T}}$ vectors is required to satisfy $m_{\mathrm{T}} < 100\,\mathrm{GeV}$. Weights are determined from simulated $\mathrm{t\bar{t}}$, W+jets, and single-top events through evaluation of the efficiency of each analysis step. Corrections are applied to account for the trigger efficiency, contamination from non-prompt electrons, contamination from dileptonic events in which one of the leptons is lost, and the selection efficiency of the $m_{\mathrm{T}}$ requirement. The number of leptonic events that fail any of the selection criteria is then evaluated by weighting the CS events with the respective acceptance, reconstruction, and isolation efficiencies. Corresponding efficiencies are evaluated for dileptonic events in which both leptons are lost. This latter source of background is predicted to account for $<$2% of the total lost-lepton background. Finally, a correction is applied to account for the selection efficiency of the isolated-track veto.

The weighted distributions of the search variables, summed over the events in the CS, define the lost-lepton background prediction. The procedure is performed separately for single-electron and single-muon events. The two independent predictions are averaged to obtain the final lost-lepton background prediction. The method is validated with a closure test, namely by determining the ability of the method, applied to simulated samples, to predict correctly the true number of background events. The results of the closure test are shown in Fig. 3 (top).

The dominant uncertainties in the lost-lepton background prediction are statistical, due to the limited number of CS events in the most sensitive search regions. As a systematic uncertainty, we take the larger of the observed non-closure in Fig. 3 (top) or the statistical uncertainty in the non-closure, for each search region. Additional systematic uncertainties are assigned based on a comparison between data and simulation of the lepton reconstruction, lepton isolation, and isolated-track-veto efficiencies. Within the statistical precision, there are no such differences observed, and the statistical uncertainty in the respective comparison is assigned as a systematic uncertainty. Uncertainties in the acceptance associated with the PDFs, including those related

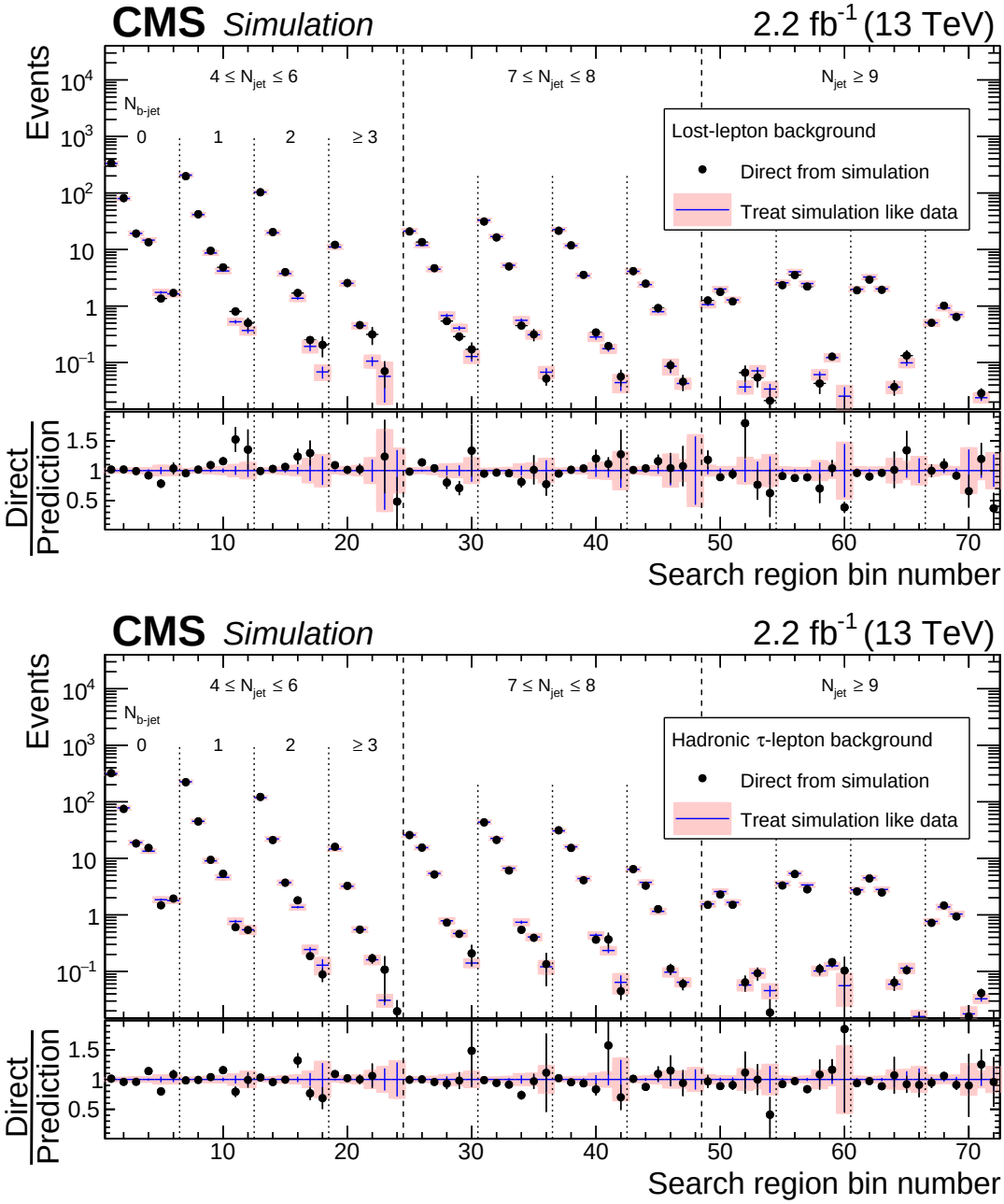


Figure 3: (top) The lost-lepton background in the 72 search regions of the analysis as predicted directly from $t\bar{t}$, single-top, and W+jets simulation (points with error bars) and as predicted by applying the lost-lepton background-determination procedure to simulated muon and electron control samples (histograms). The lower panel shows the ratio between the true and predicted yields. (bottom) The corresponding simulated results for the background from hadronically decaying $\tau$ leptons. For both plots, the six results within each region delineated by dashed lines correspond sequentially to the six regions of $H_T$ and $H_T^{miss}$ indicated in Fig. 2.

to the renormalization and factorization scales, are evaluated by varying the PDF sets used to produce the simulated samples. The uncertainty in the jet energy correction is propagated to $|\vec{p}_{\mathrm{T}}^{\,\mathrm{miss}}|$, and the effect on the $m_{\mathrm{T}}$-selection efficiency is used to define a systematic uncertainty. Small systematic uncertainties related to the purity of the muon and electron control samples and to the statistical uncertainties of the simulated efficiencies are also evaluated.

### 5.1.2 Hadronically decaying $\tau$ lepton background

To evaluate the background due to W bosons that decay to a neutrino and a hadronically decaying $\tau$ lepton ($\tau_{\mathrm{h}}$), we employ a template method [19, 52, 53]. The $\tau_{\mathrm{h}}$ background is determined from a single-muon control sample, composed almost entirely of $\mathrm{t\bar{t}}$, single-top, and W+jets events, selected using a trigger that requires $H_{\mathrm{T}} > 350\,\mathrm{GeV}$ and at least one muon candidate with $p_{\mathrm{T}} > 15\,\mathrm{GeV}$. The CS events are required to contain exactly one identified muon with $p_{\mathrm{T}} > 20\,\mathrm{GeV}$ and $|\eta| < 2.1$. Since $\mu$+jets and $\tau_{\mathrm{h}}$+jets production arise from the same underlying process, the hadronic component of the events is expected to be the same aside from the response of the detector to a $\mu$ lepton or $\tau_{\mathrm{h}}$ jet. The muon $p_{\mathrm{T}}$ in the single-muon CS is smeared according to response functions (the "templates") derived from $\mathrm{t\bar{t}}$ and W+jets simulation, which express the expected visible-$p_{\mathrm{T}}$ distribution of a $\tau_{\mathrm{h}}$ jet as a function of the true $p_{\mathrm{T}}$ value of the underlying lepton, taken to be the measured muon $p_{\mathrm{T}}$.

Following the smearing, the values of $H_{\mathrm{T}}$, $H_{\mathrm{T}}^{\mathrm{miss}}$, $N_{\mathrm{jet}}$, and $N_{\mathrm{b\text{-}jet}}$ are calculated for the CS event and the selection criteria of Section 3 are applied. The misidentification probability for a $\tau_{\mathrm{h}}$ jet to be erroneously identified as a b jet is taken into account. Corrections are applied to account for the trigger efficiency, the acceptance and efficiency of the $\mu$ selection, and the branching ratio $\mathcal{B}(\mathrm{W} \to \tau_{\mathrm{h}}\nu)/\mathcal{B}(\mathrm{W} \to \mu\nu) = 0.65$ [54]. The resulting event yield provides the $\tau_{\mathrm{h}}$ background estimate. The method is validated with a closure test, whose results are shown in Fig. 3 (bottom). Systematic uncertainties are assigned based on the level of closure, as described for the lost-lepton background. Other systematic uncertainties are associated with the muon acceptance, the response functions, and the misidentification rate of $\tau_{\mathrm{h}}$ jets as b jets. The dominant uncertainty, as for the lost-lepton background, arises from the limited statistical precision of the CS.

## 5.2 Background from $\mathrm{Z} \to \nu\bar{\nu}$ events

A straightforward method to evaluate the background from Z+jets events with $\mathrm{Z} \to \nu\bar{\nu}$ consists of selecting Z+jets events with $\mathrm{Z} \to \ell^+\ell^-$ ($\ell$ = e, $\mu$), removing the $\ell^+$ and $\ell^-$ to emulate the $\mathrm{Z} \to \nu\bar{\nu}$ process, and applying the event selection criteria of Section 3. The resulting efficiency-corrected event yields can be directly translated into a prediction for the $\mathrm{Z} \to \nu\bar{\nu}$ background through multiplication by the known branching ratio. A limitation of this procedure is the small $\mathrm{Z} \to \ell^+\ell^-$ branching fraction.

An alternative approach is to exploit the similarity between Z boson radiation and the more copious radiation of photons by selecting $\gamma$ + jets events, removing the photon from the event, and applying the selection criteria of Section 3. The $\gamma$ + jets process differs from the Z+jets process because of threshold effects associated with the Z boson mass and because of the different couplings of Z bosons and photons to up- and down-type quarks. These differences are generally well understood and can be described adequately with simulation.

Our evaluation of the $\mathrm{Z} \to \nu\bar{\nu}$ background utilizes both approaches. A $\gamma$ + jets CS is selected using a trigger that requires $H_{\mathrm{T}} > 500\,\mathrm{GeV}$ and photon $p_{\mathrm{T}} > 90\,\mathrm{GeV}$. A Z+jets CS with $\mathrm{Z} \to \ell^+\ell^-$ is selected using a trigger that requires $H_{\mathrm{T}} > 350\,\mathrm{GeV}$ and at least one electron or muon with $p_{\mathrm{T}} > 15\,\mathrm{GeV}$. Fits as in Refs. [19] and [18] are used to extract the prompt-photon and

Z boson yields, respectively. Because of the potential difference in heavy flavor production between $\gamma$ + jets and Z+jets events, we restrict the use of $\gamma$ + jets events to the 18 search regions with $N_{\text{b-jet}} = 0$. The $Z \to \ell^+\ell^-$ sample, integrated over $H_T$ and $H_T^{\text{miss}}$ because of the limited statistical precision, is used to extrapolate the $N_{\text{b-jet}} = 0$ results to the $N_{\text{b-jet}} > 0$ search regions.

The $\gamma$ + jets analysis is similar to that presented in Ref. [19]. We predict the number $N^{\text{pred}}_{Z\to\nu\bar{\nu}}$ of $Z(\to \nu\bar{\nu})$+jets events contributing to each $N_{\text{b-jet}} = 0$ search region from the number $N^{\text{data}}_{\gamma}$ of events in the corresponding $N_{\text{jet}}$, $H_T$, and $H_T^{\text{miss}}$ bin of the $\gamma$ + jets CS:

$$N^{\text{pred}}_{Z\to\nu\bar{\nu}}\Big|_{N_{\text{b-jet}}=0} = \rho \cdot \mathcal{R}_{Z\to\nu\bar{\nu}/\gamma} \cdot \beta_\gamma \cdot N^{\text{data}}_{\gamma}, \tag{1}$$

where $\beta_\gamma$ is the purity of the CS and $\mathcal{R}_{Z\to\nu\bar{\nu}/\gamma}$ the ratio from simulation of the numbers of $Z(\to \nu\bar{\nu})$+jets events to $\gamma$ + jets events, with the $\gamma$ + jets term obtained from a leading-order MADGRAPH calculation. Corrections are applied to account for the efficiency differences between the data and simulation and for an angular cutoff in the simulation that controls the singularity associated with soft collinear radiative corrections. The factor $\rho$ [19] in Eq. (1), defined as

$$\rho = \frac{\mathcal{R}^{\text{data}}_{Z\to\ell^+\ell^-/\gamma}}{\mathcal{R}^{\text{MC}}_{Z\to\ell^+\ell^-/\gamma}} = \frac{N^{\text{data}}_{Z\to\ell^+\ell^-}}{N^{\text{data}}_{\gamma}} \cdot \frac{N^{\text{MC}}_{\gamma}}{N^{\text{MC}}_{Z\to\ell^+\ell^-}}, \tag{2}$$

uses the $Z \to \ell^+\ell^-$ CS to account for potential differences in $\mathcal{R}_{Z\to\nu\bar{\nu}/\gamma}$ between simulation and data, such as those expected due to missing higher-order terms in the $\gamma$ + jets calculation, and is found to be consistent with a constant value 0.907, with uncertainties that vary with $N_{\text{jet}}$, $H_T$, and $H_T^{\text{miss}}$ between 8 and 55%.

For search regions with $N_{\text{b-jet}} > 0$, the $Z \to \nu\bar{\nu}$ background estimate is

$$\left(N^{\text{pred}}_{Z\to\nu\bar{\nu}}\right)_{j,b,k} = \left(N^{\text{pred}}_{Z\to\nu\bar{\nu}}\right)_{j,0,k} \mathcal{F}_{j,b}; \tag{3}$$

$$\mathcal{F}_{j,b} = \left(N^{\text{data}}_{Z\to\ell^+\ell^-} \cdot \beta_{\ell\ell}\right)_{0,b} / \left(N^{\text{data}}_{Z\to\ell^+\ell^-} \cdot \beta_{\ell\ell}\right)_{0,0} \cdot \mathcal{J}_{j,b}; \tag{4}$$

$$\mathcal{J}_{j,b} = N^{\text{model}}_{j,b} / N^{\text{model}}_{0,b}, \tag{5}$$

where $j$, $b$, and $k$ are bin indices (numbered from zero) for the $N_{\text{jet}}$, $N_{\text{b-jet}}$, and kinematic (i.e., $H_T$ and $H_T^{\text{miss}}$) distributions, respectively. The first term on the right-hand side of Eq. (3) is obtained from Eq. (1). The $N_{\text{b-jet}}$ extrapolation factor $\mathcal{F}$ [Eq. (4)] is obtained from the fitted $Z \to \ell^+\ell^-$ yields, with corrections to account for the $N_{\text{b-jet}}$-dependent purity $\beta_{\ell\ell}$. Other efficiencies cancel in the ratio. The dependence of the $N_{\text{b-jet}}$ shape of $\mathcal{F}$ on $N_{\text{jet}}$ is described with the factor $\mathcal{J}$ [Eq. (5)], which is taken from simulation due to the limited statistical precision of the $Z \to \ell^+\ell^-$ data. Based on studies with simulation, we determine a systematic uncertainty in $\mathcal{J}$ as follows. As a lower bound on $\mathcal{J}$, we take $N^{\text{model}}_{j,b} = N^{\text{model}}_{0,b}$, i.e., we set $\mathcal{J}_{j,b} = 1$ in Eq. (4). In this limit $\mathcal{F}$ is independent of $N_{\text{jet}}$, corresponding to a factorization of the mechanisms to produce b jets and additional jets. As an upper bound, we take $N^{\text{model}}_{j,b} = \sum_{N_{\text{jet}}\in j, N_{\text{b-jet}}\in b} \mathcal{B}(N_{\text{b-jet}}|N_{\text{jet}}; p)$, where $\mathcal{B}$ is a binomial distribution, and assume the probability $p$ for a jet to be tagged as a b jet to be independent of $N_{\text{jet}}$. This binomial behavior is expected if all tagged b jets are erroneous, i.e., not initiated by b quarks, or if the production of quarks in the hadron shower does not depend on flavor. With respect to a systematic uncertainty, the factorization and binomial extrapolations represent opposite extremes. The binomial assumption is validated in simulation; the result $p = 0.060 \pm 0.007$ is obtained from a fit to the data, of which $\simeq 0.02$ is attributable to light or charm quark jets erroneously tagged as b jets. The resulting systematic uncertainties in $\mathcal{J}$ range from a few percent to $\sim 35\%$, depending on $N_{\text{jet}}$ and $N_{\text{b-jet}}$.

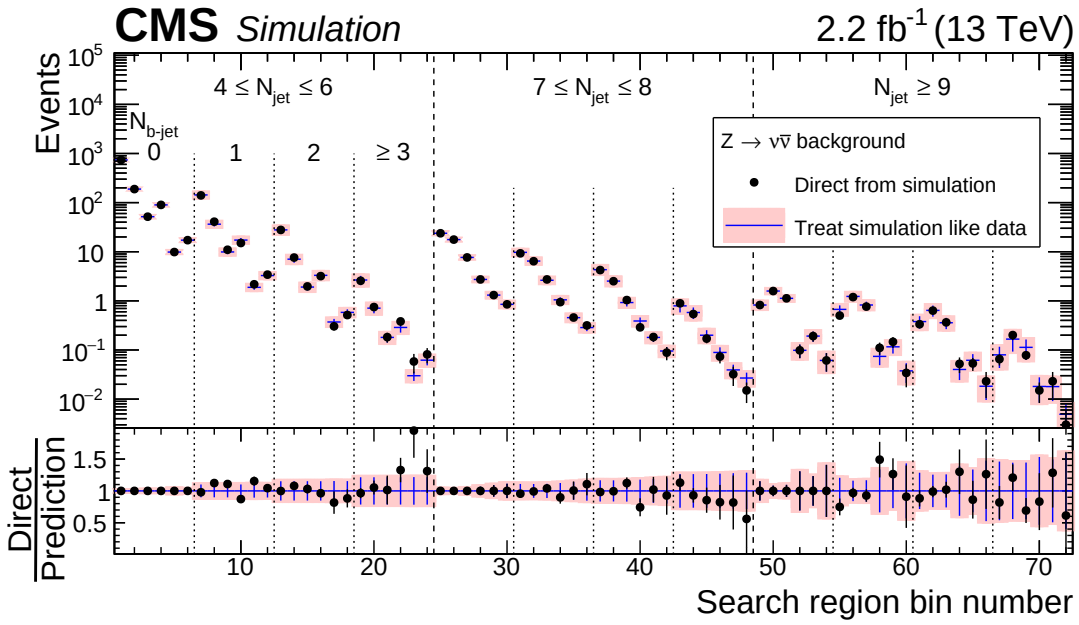


Figure 4: The $Z \to \nu\bar{\nu}$ background in the 72 search regions of the analysis as predicted directly from $Z(\to \ell^+\ell^-)$+jets and $t\bar{t}Z$ simulation (histogram), and as predicted by applying the $Z \to \nu\bar{\nu}$ background-determination procedure to simulated event samples (points with error bars). For bins corresponding to $N_{\text{b-jet}} = 0$, the agreement is exact by construction. The lower panel shows the ratio between the true and predicted yields; the shaded bands indicate the systematic uncertainty associated with the dependence of $\mathcal{F}$ on the kinematic parameters ($H_T$ and $H_T^{\text{miss}}$). The numbering of the bins is the same as in Fig. 3.

A closure test of the method is shown in Fig. 4. The shaded bands represent the systematic uncertainty (10-20%, depending on $N_{\text{b-jet}}$) arising from our treatment of $\mathcal{F}$ as independent of the kinematic parameters.

Rare processes such as $t\bar{t}Z$ and V(V)Z (V = W or Z) production can contribute to the background. We add the expectations for these processes, obtained from simulation, to the background predicted by the procedure described above. Note that processes with a Z boson and a $Z \to \gamma$ counterpart are already accounted for in $N_\gamma^{\text{data}}$ and largely cancel in the $\mathcal{R}_{Z\to\nu\bar{\nu}/\gamma}$ ratio. We find the contribution of $t\bar{t}Z$ events to be comparable to that from Z+jets events for signal regions with $N_{\text{b-jet}} \geq 2$, with an uncertainty of $\sim 50\%$. We thus add the expected yield from this process to the numerator and denominator of Eq. (5).

Besides the uncertainty related to the $N_{\text{b-jet}}$ extrapolation, discussed above, systematic uncertainties associated with the statistical precision of the simulation, the photon reconstruction efficiency, the photon and dilepton purities, and the $\rho \cdot \mathcal{R}_{Z\to\nu\bar{\nu}/\gamma}$ term are evaluated. Of these, the $\rho \cdot \mathcal{R}_{Z\to\nu\bar{\nu}/\gamma}$ term (10-55%) dominates the overall uncertainty except in the highest ($N_{\text{jet}}$, $N_{\text{b-jet}}$) search regions where the overall uncertainty is dominated by the statistical precision of the simulation (70-110%) and by the uncertainty in the $Z \to \ell^+\ell^-$ purity (60%). The underlying source of the leading systematic uncertainties is the limited number of events in the control samples.

## 5.3 Background from QCD multijet events

To evaluate the background associated with QCD multijet production, we select a QCD-dominated control sample by inverting the $\Delta\phi_{H_{\mathrm{T}}^{\mathrm{miss}},j_i}$ requirements, i.e., by requiring at least one of the four highest-$p_{\mathrm{T}}$ jets in an event to fail the respective $\Delta\phi_{H_{\mathrm{T}}^{\mathrm{miss}},j_i}$ selection criterion listed in Section 3. The resulting sample is called the "low-$\Delta\phi$" CS. The QCD background in each search region is given by the product of the observed event yield in the corresponding region of the low-$\Delta\phi$ CS multiplied by a factor $R^{\mathrm{QCD}}$ expressing the ratio of the expected QCD multijet background in the respective signal and low-$\Delta\phi$ regions, taking into account the contributions from non-QCD SM processes. The non-QCD SM contributions to the low-$\Delta\phi$ CS are evaluated using the techniques described above for the top, W+jets, and Z+jets backgrounds, except with the inverted $\Delta\phi_{H_{\mathrm{T}}^{\mathrm{miss}},j_i}$ requirements. The $R^{\mathrm{QCD}}$ terms are determined primarily from data, as described below. The procedure is analogous to that used in Refs. [18, 55] to evaluate the QCD multijet background.

For the purposes of the QCD background evaluation, we divide the $4 \leq N_{\mathrm{jet}} \leq 6$ search region into three exclusive bins: $N_{\mathrm{jet}} = 4$, 5, and 6. Once this is done, there is no dependence of $R^{\mathrm{QCD}}$ on $N_{\text{b-jet}}$. Similarly, we divide the $200 \leq H_{\mathrm{T}}^{\mathrm{miss}} \leq 500\,\mathrm{GeV}$ search region into two bins: $200 < H_{\mathrm{T}}^{\mathrm{miss}} < 300\,\mathrm{GeV}$ and $300 < H_{\mathrm{T}}^{\mathrm{miss}} < 500\,\mathrm{GeV}$. The first of these bins ($200 < H_{\mathrm{T}}^{\mathrm{miss}} < 300\,\mathrm{GeV}$) is then enhanced in QCD background, both in the low-$\Delta\phi$ and standard samples. The $H_{\mathrm{T}}$, $H_{\mathrm{T}}^{\mathrm{miss}}$, and $N_{\mathrm{jet}}$ dependence of $R^{\mathrm{QCD}}$ is modeled as:

$$R^{\mathrm{QCD}}_{i,j,k} = K^{\mathrm{QCD}}_{H_{\mathrm{T}},i} \cdot S^{\mathrm{QCD}}_{H_{\mathrm{T}}^{\mathrm{miss}},j} \cdot S^{\mathrm{QCD}}_{N_{\mathrm{jet}},k}, \tag{6}$$

where $i$, $j$ and $k$ are bin indices. The $K^{\mathrm{QCD}}_{H_{\mathrm{T}},i}$ term is the ratio of the expected number of QCD multijet events in the signal region to that in the low-$\Delta\phi$ region for $H_{\mathrm{T}}$ bin $i$ in the first $H_{\mathrm{T}}^{\mathrm{miss}}$ and $N_{\mathrm{jet}}$ bins. The $S^{\mathrm{QCD}}_{H_{\mathrm{T}}^{\mathrm{miss}},j}$ term represents a correction for $H_{\mathrm{T}}^{\mathrm{miss}}$ bin $j$ with respect to the first $H_{\mathrm{T}}^{\mathrm{miss}}$ bin, and the $S^{\mathrm{QCD}}_{N_{\mathrm{jet}},k}$ term a correction for $N_{\mathrm{jet}}$ bin $k$ with respect to the first $N_{\mathrm{jet}}$ bin. The $K^{\mathrm{QCD}}_{H_{\mathrm{T}},i}$ and $S^{\mathrm{QCD}}_{N_{\mathrm{jet}},k}$ terms are determined from a fit to data in the $200 < H_{\mathrm{T}}^{\mathrm{miss}} < 300\,\mathrm{GeV}$ bin with the non-QCD SM background taken into account. The $S^{\mathrm{QCD}}_{H_{\mathrm{T}}^{\mathrm{miss}},j}$ terms are taken from the QCD multijet simulation. Based on studies of the differing contributions of events in which the jet with the largest $p_{\mathrm{T}}$ mismeasurement is or is not amongst the four highest-$p_{\mathrm{T}}$ jets, uncertainties of 50, 100, and 100% are assigned to the $300 < H_{\mathrm{T}}^{\mathrm{miss}} < 500\,\mathrm{GeV}$, $500 < H_{\mathrm{T}}^{\mathrm{miss}} < 750\,\mathrm{GeV}$, and $H_{\mathrm{T}}^{\mathrm{miss}} \geq 750\,\mathrm{GeV}$ bins to account for potential differences between data and simulation in the $S^{\mathrm{QCD}}_{H_{\mathrm{T}}^{\mathrm{miss}},j}$ factors. Weighted results for $R^{\mathrm{QCD}}$ are calculated when recombining the $H_{\mathrm{T}}^{\mathrm{miss}}$ and $N_{\mathrm{jet}}$ results to correspond to the nominal search regions. Figure 5 presents the closure-test results for the method.

For the lowest $H_{\mathrm{T}}^{\mathrm{miss}}$ search region, the uncertainty in the prediction of the QCD multijet background is dominated by the uncertainties in $K^{\mathrm{QCD}}_{H_{\mathrm{T}},i}$ and $S^{\mathrm{QCD}}_{N_{\mathrm{jet}},k}$, which themselves are mostly due to uncertainties in the non-QCD SM background evaluated in the signal regions. For the two higher $H_{\mathrm{T}}^{\mathrm{miss}}$ search regions, the uncertainty in $S^{\mathrm{QCD}}_{H_{\mathrm{T}}^{\mathrm{miss}},j}$ and the limited statistical precision of the low-$\Delta\phi$ CS dominate the uncertainty. The uncertainties related to non-closure (Fig. 5) are negligible in comparison and are not considered.

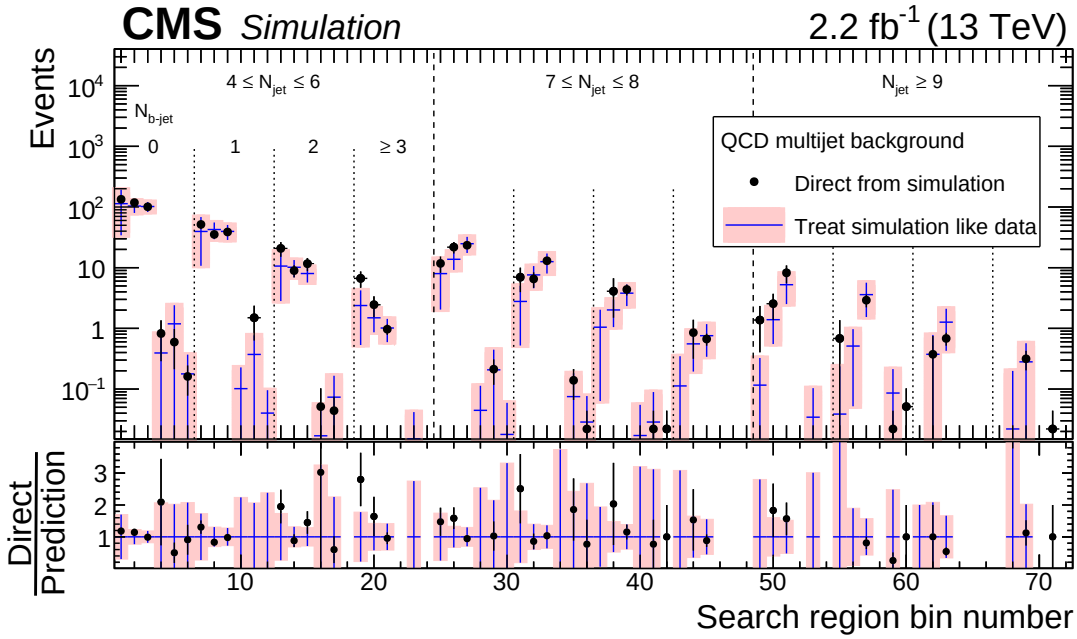


Figure 5: The QCD multijet background in the 72 search regions of the analysis as predicted directly from QCD multijet simulation (points with error bars) and as predicted by applying the QCD multijet background-determination procedure to simulated event samples (histograms). The lower panel shows the ratio between the true and predicted yields. The numbering of the bins is the same as in Fig. 3.

# 6 Results and interpretation

The observed numbers of events in the 72 search regions are shown in Fig. 6 in comparison to the predictions for the SM background. The predicted background is observed to be statistically compatible with the data in all 72 regions. Therefore, we do not observe evidence for new physics.

Figure 7 presents one-dimensional projections of the results in $H_{\mathrm{T}}^{\mathrm{miss}}$ or $H_{\mathrm{T}}$ after criteria are imposed, as indicated in the legends, to select intervals of the search-region phase space particularly sensitive to the T1bbbb, T1tttt, or T1qqqq scenarios. In each case, example distributions are shown for two signal scenarios near the respective limits of our sensitivity [18, 19] in Run 1. These scenarios, one with $m_{\tilde{\mathrm{g}}} >> m_{\tilde{\chi}_1^0}$ and one with $m_{\tilde{\chi}_1^0} \approx m_{\tilde{\mathrm{g}}}$, are excluded at 95% confidence level (CL) by the present analysis (see below).

A likelihood fit of the data is used to set limits on the production cross sections for the T1bbbb, T1tttt, and T1qqqq scenarios. The limits are determined as a function of $m_{\tilde{\chi}_1^0}$ and $m_{\tilde{\mathrm{g}}}$. The likelihood function is the product of Poisson probability density functions, one for each signal region, and constraint terms that account for statistical and systematic uncertainties. The uncertainties are treated as nuisance parameters with log-normal probability density functions. Correlations are taken into account where appropriate. The signal-model uncertainties associated with the renormalization and factorization scales, initial-state radiation, the jet energy scale, the b-jet tagging, and the statistical fluctuations vary substantially with the event kinematics and are evaluated point-by-point as a function of $m_{\tilde{\chi}_1^0}$ and $m_{\tilde{\mathrm{g}}}$. The test statistic is $q_\mu = -2\ln\left(\mathcal{L}_\mu/\mathcal{L}_{\max}\right)$, where $\mathcal{L}_{\max}$ is the maximum likelihood determined by allowing all parameters including the SUSY signal strength $\mu$ to vary, and $\mathcal{L}_\mu$ is the maximum likelihood for a fixed signal strength. To set limits, we use asymptotic results for the test statistic [56] and the

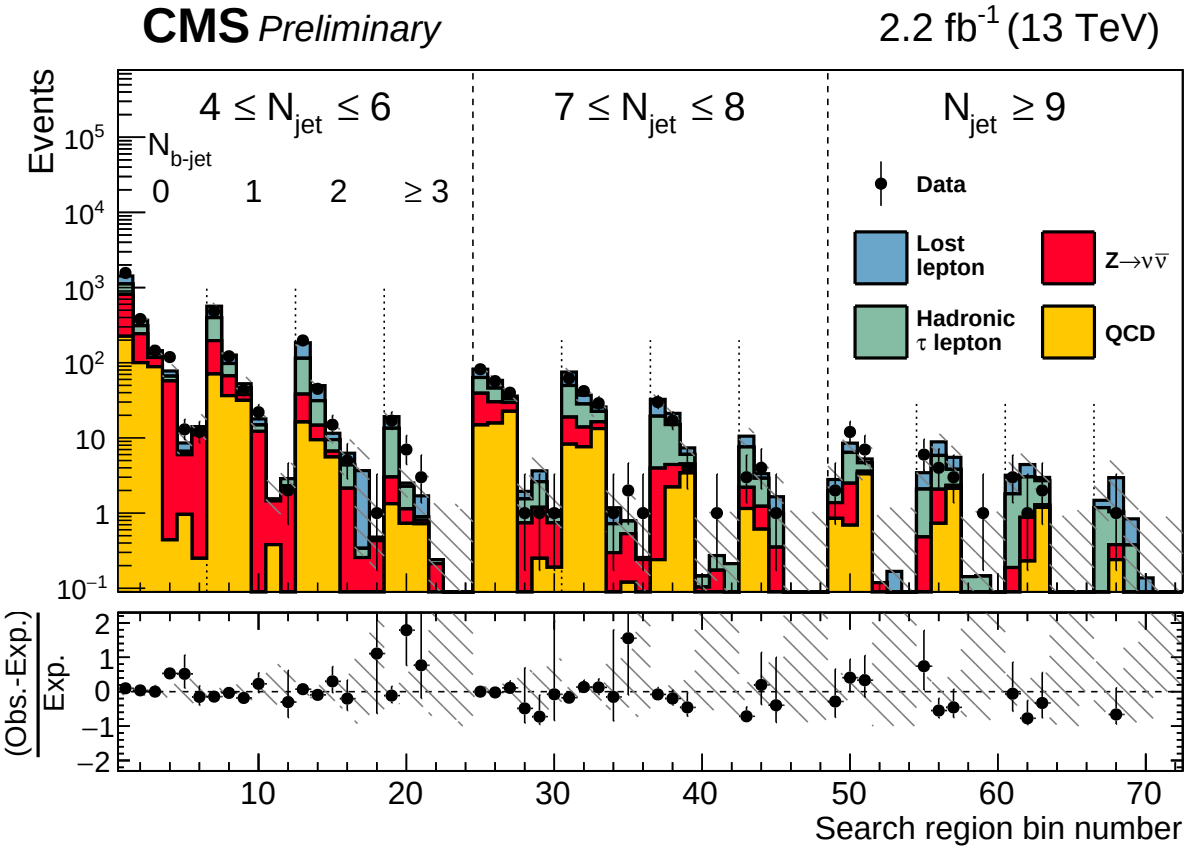


Figure 6: Observed numbers of events and corresponding SM background predictions in the 72 search regions of the analysis, with fractional differences shown in the lower panel. The hatched regions indicate the total uncertainties in the background predictions. The numbering of the bins is the same as in Fig. 3.

$CL_s$ method described in Refs. [57, 58]. More details are provided in Refs. [59, 60].

We proceed to evaluate 95% CL upper limits on the signal cross sections. The potential contributions of signal events to the control regions are taken into account when computing these limits. The NLO+NLL cross section is used as a reference to evaluate corresponding 95% CL exclusion curves. In addition to the observed limits, expected limits are derived by replacing the numbers of observed events in the signal regions with the corresponding numbers of expected background events when evaluating the test statistic. The results are shown in Fig. 8. In the limit of a massless LSP, we exclude gluinos with masses below 1600, 1530, and 1440 GeV, respectively, for the T1bbbb, T1tttt, and T1qqqq scenarios. These results significantly extend those we obtained at $\sqrt{s} = 8$ TeV, for which the corresponding limits are each around 1.15 TeV [18, 19].

## 7 Summary

A search is presented for an anomalous rate of events with four or more jets, no identified isolated electron or muon or isolated charged track, and large missing transverse momentum. The search is based on a sample of proton-proton collision data collected at $\sqrt{s} = 13$ TeV with the CMS detector at the CERN LHC in 2015, corresponding to an integrated luminosity of 2.2 $\text{fb}^{-1}$. The principal standard model backgrounds, from events with top quarks, W bosons

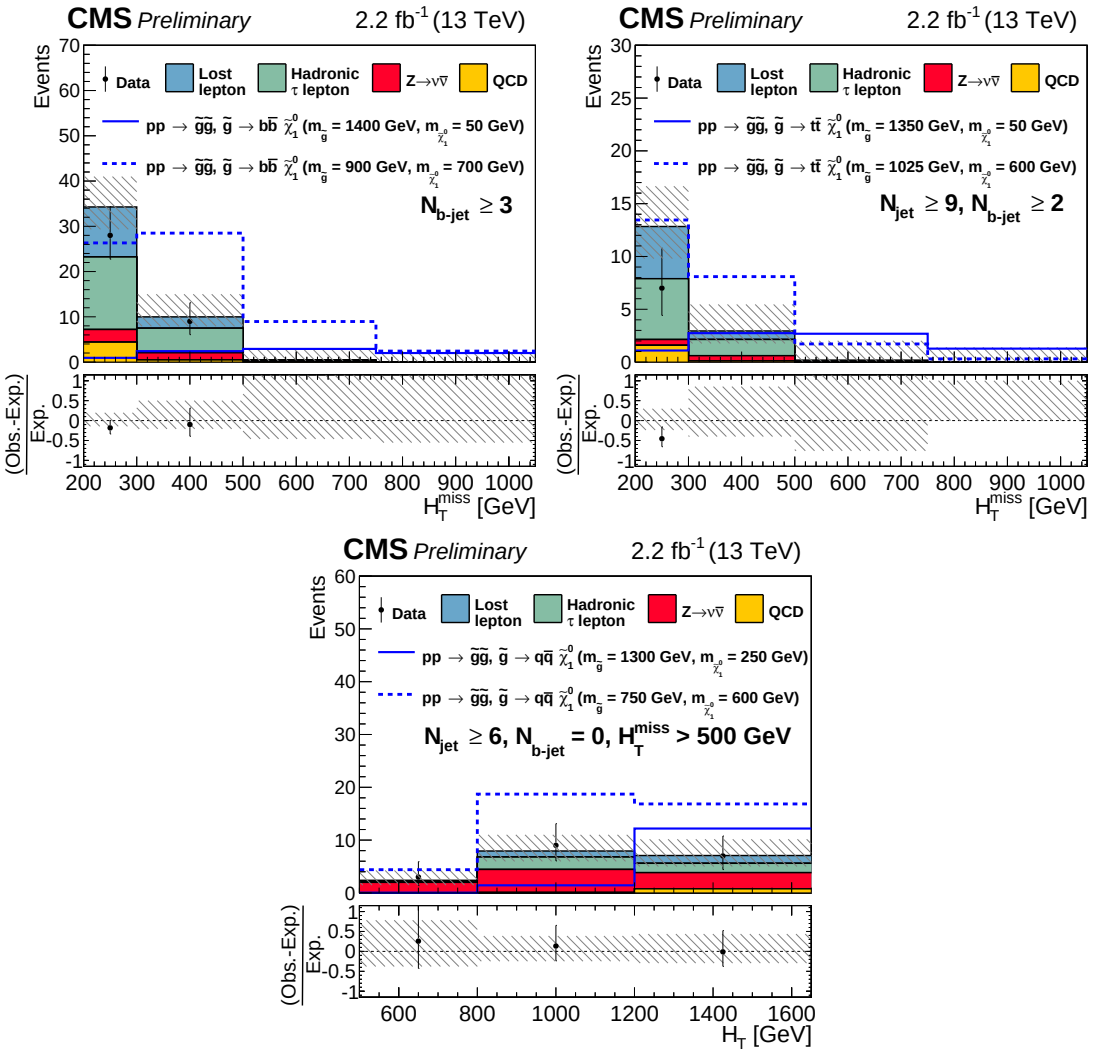


Figure 7: Observed numbers of events and corresponding SM background predictions for intervals of the search-region phase space particularly sensitive to the (top left) T1tttt, (top right) T1bbbb, and (bottom) T1qqqq scenarios. The selection requirements are given in the figure legends. The hatched regions indicate the total uncertainties in the background predictions. The (unstacked) results for two example signal scenarios are shown in each instance, one with $m_{\tilde{g}} >> m_{\tilde{\chi}^0_1}$ and the other with $m_{\tilde{\chi}^0_1} \approx m_{\tilde{g}}$. Note that for purposes of presentation, the four-bin scheme discussed in Section 5.3 is used for the $H_T^{\text{miss}}$ variable.

and jets, Z bosons and jets, and QCD multijet production, are evaluated using control samples in the data. The analysis is performed in the framework of a global likelihood fit in which the observed numbers of events in 72 exclusive bins in a four-dimensional array of missing transverse momentum, the number of jets, the number of tagged bottom-quark jets, and the scalar sum of jet $p_T$ values are compared to the standard model predictions. The standard model background estimates are found to agree with the observed numbers of events to within the uncertainties. We interpret the results in the context of simplified supersymmetry scenarios in which gluino pair production is followed by the decay of each gluino to an undetected lightest supersymmetric particle (LSP) and to a bottom quark-antiquark pair (T1bbbb model), a top quark-antiquark pair (T1tttt model), or a generic quark-antiquark pair (T1qqqq model). Using the NLO+NLL production cross section as a reference, and in the limit of a massless

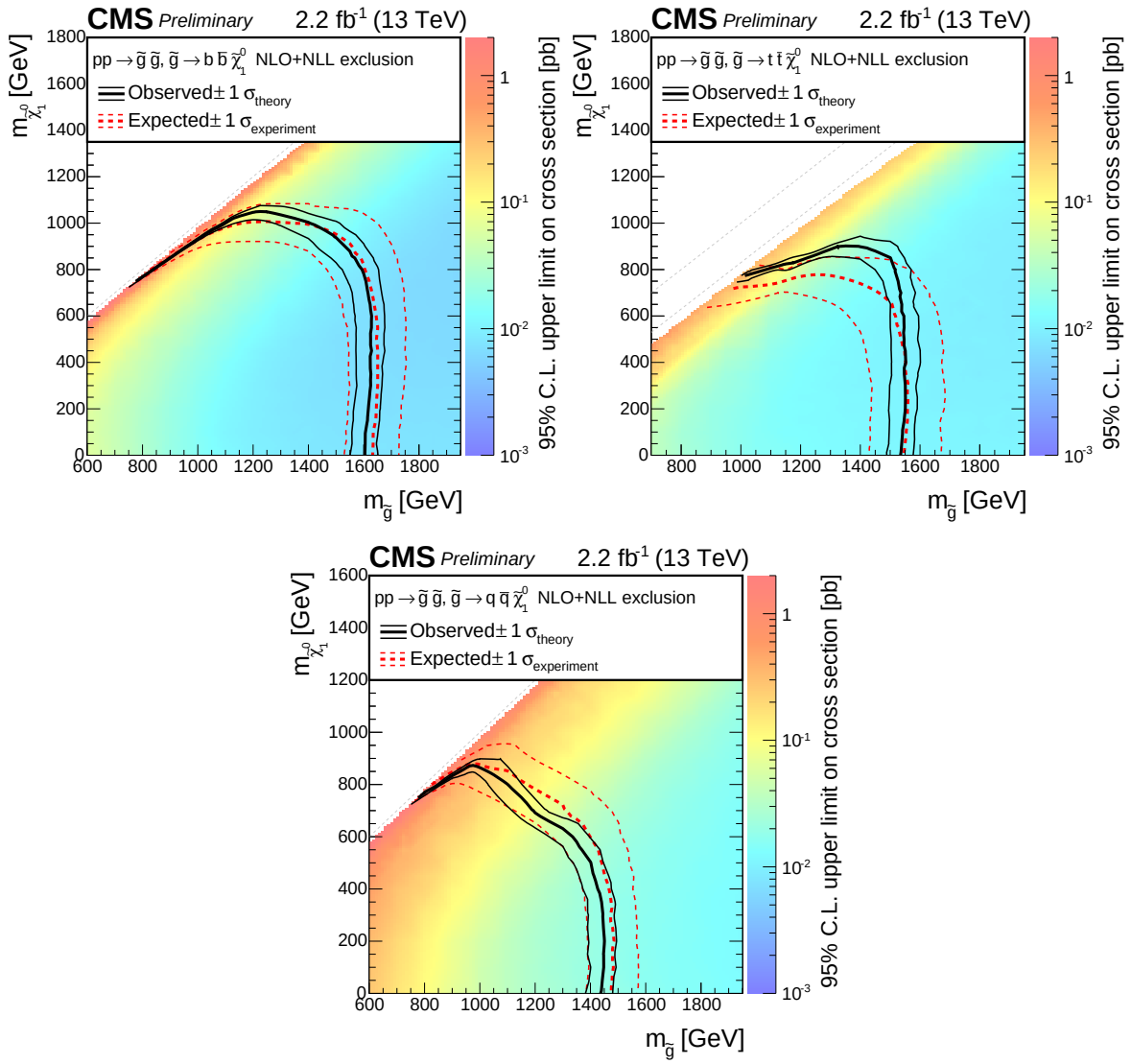


Figure 8: The 95% confidence level upper limits on the production cross sections for the (top left) T1bbbb, (top right) T1tttt, and (bottom) T1qqqq simplified model scenarios of supersymmetry, shown as a function of the gluino and LSP masses $m_{\tilde{g}}$ and $m_{\tilde{\chi}_1^0}$. The solid (black) curves show the observed exclusion contours assuming the NLO+NLL cross sections [41–45], with the corresponding $\pm 1$ standard deviation uncertainties [61]. The dashed (red) curves present the expected limits with $\pm 1$ standard deviation experimental uncertainties.

LSP, we exclude gluinos with masses below 1600, 1530, and 1440 GeV for the three scenarios, respectively, significantly extending the limits obtained in previous searches.

## References

[1] P. Ramond, "Dual theory for free fermions", *Phys. Rev. D* **3** (1971) 2415, doi:10.1103/PhysRevD.3.2415.

[2] Y. A. Golfand and E. P. Likhtman, "Extension of the algebra of Poincaré group generators and violation of P invariance", *JETP Lett.* **13** (1971) 323.

[3] A. Neveu and J. H. Schwarz, "Factorizable dual model of pions", *Nucl. Phys. B* **31** (1971) 86, doi:10.1016/0550-3213(71)90448-2.

[4] D. V. Volkov and V. P. Akulov, "Possible universal neutrino interaction", *JETP Lett.* **16** (1972) 438.

[5] J. Wess and B. Zumino, "A Lagrangian model invariant under supergauge transformations", *Phys. Lett. B* **49** (1974) 52, doi:10.1016/0370-2693(74)90578-4.

[6] J. Wess and B. Zumino, "Supergauge transformations in four dimensions", *Nucl. Phys. B* **70** (1974) 39, doi:10.1016/0550-3213(74)90355-1.

[7] P. Fayet, "Supergauge invariant extension of the Higgs mechanism and a model for the electron and its neutrino", *Nucl. Phys. B* **90** (1975) 104, doi:10.1016/0550-3213(75)90636-7.

[8] H. P. Nilles, "Supersymmetry, supergravity and particle physics", *Phys. Rep.* **110** (1984) 1, doi:10.1016/0370-1573(84)90008-5.

[9] S. Dimopoulos and G. F. Giudice, "Naturalness constraints in supersymmetric theories with nonuniversal soft terms", *Phys. Lett. B* **357** (1995) 573, doi:10.1016/0370-2693(95)00961-J, arXiv:hep-ph/9507282.

[10] R. Barbieri and D. Pappadopulo, "S-particles at their naturalness limits", *JHEP* **10** (2009) 061, doi:10.1088/1126-6708/2009/10/061, arXiv:0906.4546.

[11] M. Papucci, J. T. Ruderman, and A. Weiler, "Natural SUSY endures", *JHEP* **09** (2012) 035, doi:10.1007/JHEP09(2012)035, arXiv:1110.6926.

[12] G. R. Farrar and P. Fayet, "Phenomenology of the production, decay, and detection of new hadronic states associated with supersymmetry", *Phys. Lett. B* **76** (1978) 575, doi:10.1016/0370-2693(78)90858-4.

[13] N. Arkani-Hamed et al., "MARMOSET: The path from LHC data to the new standard model via on-shell effective theories", (2007). arXiv:hep-ph/0703088.

[14] J. Alwall, P. Schuster, and N. Toro, "Simplified models for a first characterization of new physics at the LHC", *Phys. Rev. D* **79** (2009) 075020, doi:10.1103/PhysRevD.79.075020, arXiv:0810.3921.

[15] J. Alwall, M.-P. Le, M. Lisanti, and J. G. Wacker, "Model-independent jets plus missing energy searches", *Phys. Rev. D* **79** (2009) 015005, doi:10.1103/PhysRevD.79.015005, arXiv:0809.3264.

[16] D. Alves et al., "Simplified models for LHC new physics searches", *J. Phys. G* **39** (2012) 105005, doi:10.1088/0954-3899/39/10/105005, arXiv:1105.2838.

[17] CMS Collaboration, "Interpretation of searches for supersymmetry with simplified models", (2013). arXiv:1301.2175. Submitted to *Phys. Rev. D*.

[18] CMS Collaboration, "Search for gluino mediated bottom- and top-squark production in multijet final states in pp collisions at 8 TeV", *Phys. Lett. B* **725** (2013) 243, doi:10.1016/j.physletb.2013.06.058, arXiv:1305.2390.

[19] CMS Collaboration, "Search for new physics in the multijet and missing transverse momentum final state in proton-proton collisions at $\sqrt{s}$= 8 TeV", *JHEP* **06** (2014) 055, doi:10.1007/JHEP06(2014)055, arXiv:1402.4770.

[20] CMS Collaboration, "The CMS experiment at the CERN LHC", *JINST* **3** (2008) S08004, doi:10.1088/1748-0221/3/08/S08004.

[21] CMS Collaboration, "Particle flow event reconstruction in CMS and performance for jets, taus and $E_{\mathrm{T}}^{\mathrm{miss}}$", CMS Physics Analysis Summary CMS-PAS-PFT-09-001, CERN, 2009.

[22] CMS Collaboration, "Commissioning of the particle-flow event reconstruction with the first LHC collisions recorded in the CMS detector", CMS Physics Analysis Summary CMS-PAS-PFT-10-001, CERN, 2010.

[23] CMS Collaboration, "Pileup jet identification", CMS Physics Analysis Summary CMS-PAS-JME-13-005, CERN, 2013.

[24] M. Cacciari, G. P. Salam, and G. Soyez, "The Anti-$k_t$ jet clustering algorithm", *JHEP* **04** (2008) 063, doi:10.1088/1126-6708/2008/04/063, arXiv:0802.1189.

[25] M. Cacciari, G. P. Salam, and G. Soyez, "FastJet user manual", *Eur. Phys. J. C* **72** (2012) 1896, doi:10.1140/epjc/s10052-012-1896-2, arXiv:1111.6097.

[26] M. Cacciari and G. P. Salam, "Pileup subtraction using jet areas", *Phys. Lett. B* **659** (2008) 119, doi:10.1016/j.physletb.2007.09.077, arXiv:0707.1378.

[27] CMS Collaboration, "Determination of jet energy calibration and transverse momentum resolution in CMS", *JINST* **6** (2011) P11002, doi:10.1088/1748-0221/6/11/P11002, arXiv:1107.4277.

[28] CMS Collaboration, "Identification of b-quark jets with the CMS experiment", *JINST* **8** (2013) P04013, doi:10.1088/1748-0221/8/04/P04013, arXiv:1211.4462.

[29] CMS Collaboration, "Performance of b tagging at $\sqrt{s} = 8$ TeV in multijet, $\mathrm{t\bar{t}}$ and boosted topology events", CMS Physics Analysis Summary CMS-PAS-BTV-13-001, CERN, 2013.

[30] UA1 Collaboration, "Experimental Observation of Isolated Large Transverse Energy Electrons with Associated Missing Energy at $\sqrt{s} = 540$ GeV", *Phys. Lett. B* **122** (1983) 103, doi:10.1016/0370-2693(83)91177-2.

[31] J. Alwall et al., "MadGraph5: going beyond", *JHEP* **06** (2011) 128, doi:10.1007/JHEP06(2011)128, arXiv:1106.0522.

[32] P. Nason, "A New method for combining NLO QCD with shower Monte Carlo algorithms", *JHEP* **11** (2004) 040, doi:10.1088/1126-6708/2004/11/040, arXiv:hep-ph/0409146.

[33] S. Frixione, P. Nason, and C. Oleari, "Matching NLO QCD computations with Parton Shower simulations: the POWHEG method", *JHEP* **11** (2007) 070, doi:10.1088/1126-6708/2007/11/070, arXiv:0709.2092.

[34] S. Alioli, P. Nason, C. Oleari, and E. Re, "A general framework for implementing NLO calculations in shower Monte Carlo programs: the POWHEG BOX", *JHEP* **06** (2010) 043, doi:10.1007/JHEP06(2010)043, arXiv:1002.2581.

[35] S. Alioli, P. Nason, C. Oleari, and E. Re, "NLO single-top production matched with shower in POWHEG: s- and t-channel contributions", *JHEP* **09** (2009) 111, doi:10.1007/JHEP02(2010)011,10.1088/1126-6708/2009/09/111, arXiv:0907.4076. [Erratum: JHEP02,011(2010)].

[36] E. Re, "Single-top Wt-channel production matched with parton showers using the POWHEG method", *Eur. Phys. J.* **C71** (2011) 1547, doi:10.1140/epjc/s10052-011-1547-z, arXiv:1009.2450.

[37] J. Alwall et al., "The automated computation of tree-level and next-to-leading order differential cross sections, and their matching to parton shower simulations", *JHEP* **07** (2014) 079, doi:10.1007/JHEP07(2014)079, arXiv:1405.0301.

[38] T. Melia, P. Nason, R. Rontsch, and G. Zanderighi, "W+W-, WZ and ZZ production in the POWHEG BOX", *JHEP* **11** (2011) 078, doi:10.1007/JHEP11(2011)078, arXiv:1107.5051.

[39] S. Agostinelli et al., "GEANT4 — a simulation toolkit", *Nucl. Instr. and Meth. A* **506** (2003) 250, doi:10.1016/S0168-9002(03)01368-8.

[40] T. Sjöstrand et al., "An Introduction to PYTHIA 8.2", *Comput. Phys. Commun.* **191** (2015) 159–177, doi:10.1016/j.cpc.2015.01.024, arXiv:1410.3012.

[41] W. Beenakker, R. Höpker, M. Spira, and P. M. Zerwas, "Squark and gluino production at hadron colliders", *Nucl. Phys. B* **492** (1997) 51, doi:10.1016/S0550-3213(97)00084-9, arXiv:hep-ph/9610490.

[42] A. Kulesza and L. Motyka, "Threshold resummation for squark-antisquark and gluino-pair production at the LHC", *Phys. Rev. Lett.* **102** (2009) 111802, doi:10.1103/PhysRevLett.102.111802, arXiv:0807.2405.

[43] A. Kulesza and L. Motyka, "Soft gluon resummation for the production of gluino-gluino and squark-antisquark pairs at the LHC", *Phys. Rev. D* **80** (2009) 095004, doi:10.1103/PhysRevD.80.095004, arXiv:0905.4749.

[44] W. Beenakker et al., "Soft-gluon resummation for squark and gluino hadroproduction", *JHEP* **12** (2009) 041, doi:10.1088/1126-6708/2009/12/041, arXiv:0909.4418.

[45] W. Beenakker et al., "Squark and gluino hadroproduction", *Int. J. Mod. Phys. A* **26** (2011) 2637, doi:10.1142/S0217751X11053560, arXiv:1105.1110.

[46] CMS Collaboration, "Fast simulation of the CMS detector", *J. Phys. Conf. Ser.* **219** (2010) 032053, doi:10.1088/1742-6596/219/3/032053. (D. Orbaker for the collaboration).

[47] CMS Collaboration, "Comparison of the fast simulation of CMS with the first LHC data", CMS Detector Performance Summary CMS-DP-2010-039, CERN, 2010.

[48] NNPDF Collaboration, "Parton distributions for the LHC Run II", *JHEP* **04** (2015) 040, doi:10.1007/JHEP04(2015)040, arXiv:1410.8849.

[49] S. Catani, D. de Florian, M. Grazzini, and P. Nason, "Soft gluon resummation for Higgs boson production at hadron colliders", *JHEP* **07** (2003) 028, doi:10.1088/1126-6708/2003/07/028, arXiv:hep-ph/0306211.

[50] M. Cacciari et al., "The t anti-t cross-section at 1.8-TeV and 1.96-TeV: A Study of the systematics due to parton densities and scale dependence", *JHEP* **04** (2004) 068, doi:10.1088/1126-6708/2004/04/068, arXiv:hep-ph/0303085.

[51] CMS Collaboration, "Search for top-squark pair production in the single-lepton final state in pp collisions at $\sqrt{s}$ = 8 TeV", *Eur. Phys. J. C* **73** (2013) 2677, doi:10.1140/epjc/s10052-013-2677-2, arXiv:1308.1586.

[52] CMS Collaboration, "Search for New Physics with Jets and Missing Transverse Momentum in pp collisions at $\sqrt{s} = 7$ TeV", *JHEP* **08** (2011) 155, doi:10.1007/JHEP08(2011)155, arXiv:1106.4503.

[53] CMS Collaboration, "Search for new physics in the multijet and missing transverse momentum final state in proton-proton collisions at $\sqrt{s} = 7$ TeV", *Phys. Rev. Lett.* **109** (2012) 171803, doi:10.1103/PhysRevLett.109.171803, arXiv:1207.1898.

[54] Particle Data Group, K. A. Olive et al., "Review of particle physics", *Chin. Phys. C* **38** (2014) 090001, doi:10.1088/1674-1137/38/9/090001.

[55] CMS Collaboration, "Search for supersymmetry in events with b-quark jets and missing transverse energy in pp collisions at 7 TeV", *Phys. Rev. D* **86** (2012) 072010, doi:10.1103/PhysRevD.86.072010, arXiv:1208.4859.

[56] G. Cowan, K. Cranmer, E. Gross, and O. Vitells, "Asymptotic formulae for likelihood-based tests of new physics", *Eur. Phys. J. C* **71** (2011) 1554, doi:10.1140/epjc/s10052-011-1554-0, 10.1140/epjc/s10052-013-2501-z, arXiv:1007.1727. [Erratum: Eur. Phys. J.C73,2501(2013)].

[57] T. Junk, "Confidence level computation for combining searches with small statistics", *Nucl. Instr. and Meth. A* **434** (1999) 435, doi:10.1016/S0168-9002(99)00498-2, arXiv:hep-ex/9902006.

[58] A. L. Read, "Presentation of search results: the $CL_s$ technique", *J. Phys. G* **28** (2002) 2693, doi:10.1088/0954-3899/28/10/313.

[59] ATLAS and CMS Collaborations, "Procedure for the LHC Higgs boson search combination in Summer 2011", Technical Report CMS-NOTE-2011-005, ATL-PHYS-PUB-2011-11, 2011.

[60] CMS Collaboration, "Searches for Supersymmetry using the $M_{T2}$ Variable in Hadronic Events Produced in pp Collisions at 8 TeV", *JHEP* **05** (2015) 078, doi:10.1007/JHEP05(2015)078, arXiv:1502.04358.

[61] M. Krämer et al., "Supersymmetry production cross sections in pp collisions at $\sqrt{s} = 7$ TeV", (2012). arXiv:1206.2892.